



Horizontal advection, diffusion, and plankton spectra at the sea surface

Annalisa Bracco,¹ Sophie Clayton,^{2,3} and Claudia Pasquero⁴

Received 3 December 2007; revised 13 September 2008; accepted 24 November 2008; published 4 February 2009.

[1] Plankton patchiness is ubiquitous in the oceans, and various physical and biological processes have been proposed as its generating mechanisms. However, a coherent statement on the problem is missing, because of both a small number of suitable observations and an incomplete understanding of the properties of reactive tracers in turbulent media. It has been suggested that horizontal advection may be the dominant process behind the observed distributions of phytoplankton and zooplankton, acting to mix tracers with longer reaction times (R_t) down to smaller scales. Conversely, the relative distributions of sea surface temperature and phytoplankton has been attributed to small-scale upwelling, where tracers with longer R_t are able to homogenize more than those with shorter reaction times. Neither of the above mechanisms can explain simultaneously the (relative) spectral slopes of temperature, phytoplankton, and zooplankton. Here, with a simple advection model and a large suite of numerical experiments, we concentrate on some of the physical processes influencing the relative distributions of tracers at the ocean surface, and we investigate (1) the impact of the spatial scale of tracer supply, (2) the role played by coherent eddies on the distribution of tracers with different R_t , and (3) the role of diffusion (so far neglected). We show that diffusion determines the distribution of temperature, regardless of the nature of the forcing. We also find that coherent structures together with differential diffusion of tracers with different R_t impact the tracer distributions. This may help in understanding the highly variable nature of observed plankton spectra.

Citation: Bracco, A., S. Clayton, and C. Pasquero (2009), Horizontal advection, diffusion, and plankton spectra at the sea surface, *J. Geophys. Res.*, 114, C02001, doi:10.1029/2007JC004671.

1. Introduction

[2] Spatial heterogeneity in the distribution of phytoplankton and zooplankton impacts ecosystem stability (see, for example, Steele [1974]), diversity [Bracco *et al.*, 2000a] and regional productivity [Lévy *et al.*, 2001b; Martin *et al.*, 2002; Pasquero *et al.*, 2005]. It is therefore important to investigate the processes responsible for generating patchiness in order to better understand the oceanic ecosystem as a whole. The ready availability of observational data thanks to improved sampling techniques and high-resolution remote sensing tools, as well as high-resolution ocean-biological models which can resolve mesoscale and submesoscale features, have led to a proliferation of studies investigating the interplay between oceanic flows and ecosystem dynamics [e.g., Falkowski *et al.*, 1991; McGillicuddy *et al.*, 1998; Oschlies and Garçon, 1998; Abraham, 1998; Spall and

Richards, 2000; Mahadevan and Archer, 2000; Martin *et al.*, 2002; Pasquero *et al.*, 2005; McGillicuddy *et al.*, 2007].

[3] Remote sensing has proved a useful tool in observing the spatial distribution of tracers at the sea surface, in particular sea surface temperature and chlorophyll *a*, and has complemented the numerous in situ observations of phytoplankton, zooplankton and temperature taken along ship transects. Mackas and Boyd [1979] were the first to employ spectral analysis to compare simultaneous spatial distributions of phytoplankton, zooplankton and temperature in the North Sea. They found that at scales of 10–100 km, zooplankton had a more patchy distribution than phytoplankton, hence a flatter spectral slope (about -1.2 for zooplankton versus -1.5 to -1.7 for phytoplankton), and that temperature had the steepest spectral slope of all (close to -2), indicating the least patchy distribution. Several other observational studies have confirmed this general behavior [Horwood, 1981; Weber *et al.*, 1986; Levin *et al.*, 1989; Tsuda *et al.*, 1993]. However, a field survey by Piontkovski *et al.* [1997] in open ocean regions of the Atlantic, Indian Ocean and Adriatic Sea and a more recent work by Martin and Srokosz [2002], analyzing transects in the North Atlantic, found similar results for temperature, but a more variable relationship between phytoplankton and zooplankton spectra. Piontkovski *et al.* [1997] noted very similar slopes for the various planktonic species, ranging between -2 and -3 in a band of wavelengths between 10 and 100 km, in the absence of

¹EAS-CNS, Georgia Institute of Technology, Atlanta, Georgia, USA.

²MIT/WHOI Joint Program in Oceanography, Department of Physical Oceanography, Woods Hole Oceanographic Institution, Woods Hole, Massachusetts, USA.

³Department of Earth, Atmospheric, and Planetary Sciences, Massachusetts Institute of Technology, Cambridge, Massachusetts, USA.

⁴Department of Earth System Science, University of California, Irvine, California, USA.

large-scale blooms. *Martin and Srokosz* [2002] observed zooplankton and phytoplankton distributions about a week after a bloom in a region of intense mesoscale activity. Zooplankton were separated into different size classes and in some cases had a steeper spectral slope than phytoplankton, but there was no obvious relationship between zooplankton size and their distribution [see *Martin and Srokosz*, 2002, Figure 2], with all the slopes lying between -1 and -1.5 .

[4] Several processes, both physical and biological, may induce this spatial heterogeneity. The main debate in patchiness studies has been centered on whether physical or biological processes are responsible for the observed distributions of phytoplankton and zooplankton. Horizontal advection [*Abraham*, 1998; *Bracco et al.*, 2000a], low-frequency variability intrinsic to mesoscale dynamics [*Levy and Klein*, 2004], biological interactions [*Denman et al.*, 1977; *Folt and Burns*, 1999] and vertical advection at the mesoscale and submesoscales have all been suggested as generating mechanisms [*Mahadevan and Archer*, 2000; *Lévy et al.*, 2001b; *Mahadevan and Campbell*, 2002; *Mahadevan and Tandon*, 2006]. All of the above processes operate on different spatial and timescales, and may affect different tracers in different ways as a function of the reaction time of the tracer.

[5] At the mesoscale and submesoscale, ocean dynamics are dominated by the presence of eddies and fronts. Coherent structures are instrumental in the upwelling of nutrients from below the mixed layer [*Falkowski et al.*, 1991; *McGillicuddy and Robinson*, 1997; *Siegel et al.*, 1999; *McGillicuddy et al.*, 2007; *Koszalka*, 2008], act as transport barriers over long periods of time [*Provenzale*, 1999], and are important in generating strong dispersive strain regions in the areas between them [*Elhmaïdi et al.*, 1993; *Bracco et al.*, 2004].

[6] The role of horizontal stirring and mixing induced by mesoscale vortices on the planktonic ecosystem was first investigated by *Abraham* [1998], who coupled a simple biological model to a two-dimensional turbulent flow. There was no explicit diffusive term in this model and numerical diffusion was neglected. *Abraham* [1998] considered three tracers with varying reaction times: carrying capacity, phytoplankton, and zooplankton. They were input at the large scale with their carrying capacity continually relaxing toward a meridionally varying background value. In the resulting spectra, zooplankton had a flatter slope than phytoplankton. This was attributed to their different reaction times. Zooplankton have a longer reaction time than phytoplankton, and consequently more time to be mixed down to finer spatial scales by the turbulent flow. Changing the biological parameters of the model does result in some variation in the spectra, but, in most realistic cases, phytoplankton conserve a steeper slope than zooplankton. This suggests that whenever the nutrient is supplied at scales of few hundreds of kilometers or larger, horizontal advection is the dominant process in generating the observed distributions of the planktonic tracers.

[7] Sea surface temperature (SST) can be considered as a passive tracer with a relatively long reaction time, determined by the response of the mixed layer temperature to changes in the air-sea heat fluxes. A qualitative estimate of the response time of SST (R_{t-SST}) can be obtained considering that $R_{t-SST} \propto \frac{\Delta T \rho h C_p}{Q}$, where ΔT is an underlying typical SST anomaly, ρ is the seawater density, C_p its specific heat capacity, h is the

depth of the mixed layer, and Q the heat flux per unit surface. This provides a bulk estimate of the order of a few months and the reader should bear in mind that we are interested in a qualitative assessment (see *Park et al.* [2005] for an estimate based on observations). In the following we will assume $R_{t-SST} \approx 40$ days, as in the paper by *Mahadevan and Campbell* [2002], using $\Delta T \sim 1$ K, $h \sim 50$ m, $Q \sim 50$ W m $^{-2}$. Following *Abraham* [1998], temperature would have a very patchy distribution, patchier than zooplankton, as a result of its longer reaction time. In reality, SST distributions are characterized by a spectral slope close to -2 at scales of 1–100 km. Other processes must therefore be implicated in generating observed SST distributions.

[8] A later study by *Mahadevan and Campbell* [2002] sought to explain the relative distributions of SST and chlorophyll a by analyzing simultaneous satellite images of the two tracers. They analyzed the variance of these tracers at different spatial scales and confirmed that SST does indeed have a less patchy distribution than chlorophyll a . They extended their study using a 3-D primitive equation model of a frontal region. The ocean mixed layer was supplied with tracers of varying reaction times by the modeled vertical velocity. The tracer corresponding to phytoplankton (with short R_t) exhibited a patchier distribution than the tracer with a reaction time of 40 days, representative of SST. The authors attributed this behavior to the fact that whenever the input is at the small scale, tracers with longer R_t have more time to homogenize, thus transferring variance from small to large scales. Diffusion is not accounted for in their interpretation of the results, although this process is represented in the model. Finally, *Levy and Klein* [2004] pointed out that the intrinsic low-frequency variability of the ocean mesoscale can cause the spectra of the vorticity to vary in time. The concentrations of phytoplankton and zooplankton are intimately associated to the relative vorticity patterns, as plankton tends to be more abundant within eddies and filaments, and therefore changes in the spectral slope of plankton will follow those of vorticity.

[9] Building upon the studies above, the aim of this work is to reconcile the results of *Abraham* [1998] and *Mahadevan and Campbell* [2002], and to further investigate the role of (1) horizontal advection for different spatial scales of tracer supply to the surface; (2) diffusion, which has been neglected so far; and (3) coherent structures such as eddies and filaments, on the distribution of tracers with different R_t .

[10] We do so by adopting a two-dimensional quasigeostrophic model to numerically simulate the ocean mesoscale turbulence and we focus on scales of 2–200 km, where the quasigeostrophic approximation is valid and our results can be directly compared to those of *Abraham* [1998] and *Mahadevan and Campbell* [2002]. Despite its simplicity and limitations, this model allows for the separation of the respective roles of horizontal advection, localized tracer supply, and diffusion.

[11] We characterize the tracer distributions using spectral analysis, as it is the most widely applied tool for investigating plankton patchiness since the 1970s (see for example *Platt* [1972], *Mackas and Boyd* [1979], *Gower et al.* [1980], *Weber et al.* [1986], *Tsuda et al.* [1993], *Powell and Okubo* [1994], *Abraham* [1998], and *Martin and Srokosz* [2002]). Although spectral analysis has numerous drawbacks, including the reduction of a complex spatial system to a single number [*Armi and Flament*, 1985; *Martin and Srokosz*, 2002], and

the assumption of isotropy in the distribution [Mahadevan and Campbell, 2002], it is still used to quantify the heterogeneity in collected data, and to test model performance and working hypotheses on plankton patchiness.

2. Model

[12] In the ocean, mesoscale advection processes and planktonic reactions occur on timescales of the same order of magnitude, leading to a significant interplay between physical and biological dynamics and a lack of temporal scale separation between them. In order to investigate this interplay, we use a simple quasigeostrophic (QG) barotropic model that we take as a first approximation to the ocean mesoscale turbulence, away from coastal boundaries [Salmon, 1998]. The statistical properties of horizontal velocities and horizontal transport and mixing in the ocean are well described by QG turbulence [e.g., Bracco et al., 2000b, 2000c, 2004]. This has been verified by using a 3-D primitive equation model by Koszalka [2008]. Fronts are not represented in QG flows, but they do not modify the horizontal velocity statistics, as shown by Schorghofer [2000] using the surface quasi-geostrophic approximation. The QG advection model resolves vortices and filaments in detail but does not allow for an explicit representation of upwelling and downwelling events, because vertical velocities are not included in the calculations. Additionally, mixed layer dynamics, which may play an important role in generating sea surface spatial variability, are not represented. The simplicity of the model, on the other hand, allows for investigating the role of the reaction timescale, horizontal diffusion and tracer supply (imposed upwelling) configurations for a broad range of parameters. The use of a 3-D, baroclinic QG turbulent model would provide analogous results, since dispersion properties in barotropic and baroclinic turbulence are very similar [Bracco et al., 2004]. A fully 3-D primitive equation model would improve the realism of this work, as the upwelling would not have to be prescribed but would be induced by the (modeled) vertical velocities. However, that approach would not allow us to perform the large number of experiments necessary to investigate the role of diffusion, the scale of the tracer supply and the presence of coherent structures. Finally, the comparison of experiments with the same horizontal flow and different upwelling setups would not be possible.

[13] The evolution equation of an incompressible, stationary QG barotropic flow is given by

$$\frac{\partial \omega}{\partial t} + [\psi, \omega] = D + F \quad (1)$$

where ψ is the stream function and $\omega = \Delta \psi$ is relative vorticity. The square brackets indicate the two-dimensional Jacobian operator, and F and D are forcing and dissipation terms, respectively. Dissipation is given by the sum of a hyperviscosity term acting at small scales, $D_S = -\nu_S \nabla^8 \nabla^2 \psi$, and of a hypoviscosity term, $D_L = +\nu_L \nabla^{-2} \nabla^2 \psi$, that removes energy at large scales. The latter represents a frictional brake and avoids energy accumulation at large scales. Forcing is obtained by keeping the amplitude of the energy power

spectrum fixed at a wave number $k_F = 10$, while allowing the phase to evolve dynamically. This forcing allows for vortex formation, but breaks spatial correlations at scales larger than about $1/k_F$. As a result, the size of the coherent vortices is constrained between the dissipation and the forcing scales, but no larger than the latter. Equation (1) is integrated numerically using a pseudo-spectral code and a third-order Adams-Bashforth time integration scheme in a doubly periodic domain. The spatial resolution is 0.5 km, the domain size L is 256 km \times 256 km and the forcing scale is 25 km. (The effective resolution of the model is about 1 km, because of the smoothing associated with the dealiasing. This is below the range where quasigeostrophic dynamics provides an adequate description of the ocean turbulence. Such a high resolution is used only for assuring numerical convergence of the solution and smoothness of the flow field below the scale of few kilometers.) The forcing strength and viscosity coefficients have been chosen so that the resolved mesoscale velocity field has eddy kinetic energy of $8 \times 10^{-4} \text{ m}^2 \text{ s}^{-2}$, and constant rate of long time dispersion, or eddy diffusivity, of $1200 \text{ m}^2 \text{ s}^{-1}$, consistent with the estimates of Ledwell et al. [1998] and Sundermeyer and Price [1998] for the North Atlantic. The model eddy diffusivity is calculated from the dispersion of 512^2 Lagrangian tracers, advected by the turbulent flow. Further details on the model can be found in the paper by Pasquero et al. [2004].

[14] The equations describing a generic active tracer or a more complex Nutrient-Phytoplankton-Zooplankton (NPZ) system are embedded in the QG model. In the following, we first analyze the distribution of a generic reactive tracer described by the equation

$$\frac{dC}{dt} = \frac{\partial C}{\partial t} + [\psi, C] = \frac{1}{R_t} [C_0(x, y) - C(x, y)] + \lambda \nabla^2 C. \quad (2a)$$

Here $\frac{1}{R_t}(C_0 - C)$ represents a source term for a tracer C with a given relaxation time R_t and spatial distribution $C_0(x, y)$. $1/R_t$ is the tracer relaxation rate to a background concentration $C_0(x, y)$, and $\lambda \nabla^2 C$ parameterizes turbulent diffusion at scales below the model resolution, according to Fick's law (see Appendix A for more details).

[15] In the next section we will focus primarily on the generic tracer described by equation (2a). Analogous results have been obtained by implementing a more complex reaction model for the tracer evolution, indicated as Phytoplankton-Zooplankton (PZ) in the rest of the paper. This model stems from the one introduced by Abraham [1998] and consists of three equations coupling a carrying capacity field, described in equation (2a), to the evolution of phytoplankton and zooplankton concentrations as

$$\frac{dP}{dt} = g(C, P, Z) + \lambda' \nabla^2 P = P(1 - P/C) - PZ + \lambda' \nabla^2 P \quad (2b)$$

$$\begin{aligned} \frac{dZ}{dt} &= h(C, P, Z) + \lambda'' \nabla^2 Z \\ &= \gamma P(t - \tau) Z(t - \tau) - \mu_Z Z^2 + \lambda'' \nabla^2 Z. \end{aligned} \quad (2c)$$

The phytoplankton growth is logistic (first term rhs in equation 2b) and controlled by the carrying capacity, and

grazing is represented by a simple PZ term. γ is the assimilation efficiency for zooplankton. A delay period τ is introduced ad hoc in the assimilation term to represent the maturation time of zooplankton, and $\mu_Z Z^2$ represents zooplankton mortality. The use of different values for the diffusion coefficients of C, P and Z will be justified below.

[16] Finally, we further confirm our analysis using the standard formulation of the Nutrient-Phytoplankton-Zooplankton (NPZ) dynamics proposed by *Fasham et al.* [1990] and widely used in the literature [i.e., *Oschlies and Garcon*, 1998, 1999; *Martin et al.*, 2002; *Pasquero et al.*, 2005]. This model is described in Appendix B.

2.1. Spatial Scale of Tracer Supply

[17] First, we investigate the impact of the spatial scale of tracer supply using the tracer equation (2a). We assume that the concentration of C relaxes to a background value that depends on a constant and abundant reservoir, C_0 , according to $\frac{1}{R_t}[C_0(x, y) - C(x, y)]$, in the following configurations:

[18] 1. $C_0 = [1 - \cos(2\pi y/L)] [1 - \cos(2\pi x/L)]/2$; In this configuration the tracer is introduced at the domain scale L in a circular patch. This is representative of large-scale nutrient gradients generated, for instance, by mixed layer entrainment or wind-driven upwelling.

[19] 2. $C_0 = [1 - \cos(64 \times 2\pi y/L)] [1 - \cos(64 \times 2\pi x/L)]/2$; The tracer is introduced in small patches evenly distributed over the domain, with no correlation to the flow field. This represents the most unrealistic of the supply regimes considered. It does allow, however, for the investigation of whether or not the scale of the upwelling, per se, may influence the power spectra of the tracer distributions.

[20] 3. $C_0 = C_A = 1$ inside vortices and filaments and $C_0 = C_N = 0$ in the background turbulence. (Analogous results have been obtained for $0 < C_N = C_A$, with ratios of C_A/C_N from 10 to 100, representative of the expected range of upwelling amplification in coherent structures in the open ocean [see, e.g., *Martin and Richards*, 2001; *McGillicuddy et al.*, 2007]).

[21] In short, we consider the following: large-scale supply events as in the paper by *Abraham* [1998], small-scale supply decorrelated with the flow field, and localized tracer input within coherent structures.

2.2. (Turbulent) Diffusivity Coefficient

[22] Diffusion of the biochemical tracers in our model is intended to represent the effects of subgrid-scale processes, i.e., dynamical features smaller than 1 km. In choosing the value of the diffusivity coefficient λ , we follow the NATRE estimates (NATRE) [*Ledwell et al.*, 1998; *Polzin*, 2003; *Polzin and Ferrari*, 2004]. In smooth flows the spreading rate of a tracer is regulated by its reaction timescale, and the diffusivity coefficient for a reactive tracer is a function of R_t [*Plumb*, 1979; *Pasquero*, 2005; *Richards and Brentnall*, 2006]. If a biochemical tracer reacts on timescales of the order of, or shorter than, the Lagrangian decorrelation time of the flow, it will not experience the constant spreading rate characteristic of the Brownian regime. As a result, tracers reacting quickly will spread less than those reacting more slowly. In order to allow for this effect, a different effective diffusivity for each tracer should be used.

[23] We adopt an effective diffusivity of $1 \text{ m}^2 \text{ s}^{-1}$ for SST, assuming that the adjustment time of the mixed layer temperature to anomalous air-sea heat fluxes is about 40 days as in the paper by *Mahadevan and Campbell* [2002], which is much larger than the Lagrangian decorrelation time of the flow (about two weeks in the ocean and in the modeled flow). Zooplankton mature in about 10–14 days and thus experience a smaller effective eddy diffusivity; we use $\lambda = 0.5 \text{ m}^2 \text{ s}^{-1}$ for zooplankton choosing a representative $R_t = 12$ days. Finally, phytoplankton is characterized by a reaction time of 2–5 days, so we adopt $\lambda = 0.05 \text{ m}^2 \text{ s}^{-1}$, corresponding to $R_t = 4$ days. The values of λ are calculated from the dispersion curves of stochastic processes with statistical properties analogous to those of the flow trajectories during the NATRE experiment. We also consider the case with no diffusivity ($\lambda = 0$), and a few other eddy diffusivity coefficients between 0 and $1 \text{ m}^2 \text{ s}^{-1}$.

3. Results

[24] We concentrate on the distribution spectra of the generic reactive scalar described by equation (2a) for various diffusion coefficients, relaxation timescales, and the three supply scenarios (large-scale, small-scale, and within coherent structures). Despite the simplicity of the scalar field equation, useful information can be drawn from this exercise.

3.1. Large-Scale Supply

[25] As in the paper by *Abraham* [1998], when the tracer supply is at the large scale in the absence of diffusion the spectral slope of the tracer distribution is determined by the relaxation time R_t . For long R_t the scalar has time to cascade to small scales and develops increasingly fine structure, which results in a flatter spectrum (see Figure 1). For a reactive scalar relaxing to the background concentration with a characteristic time of about 4 days (as for phytoplankton), the spectral slope at scales of 2–200 km is ~ -2.5 . The slope flattens to -2.1 for a relaxation time of about two weeks (as for zooplankton), and to -1.3 if R_t is of the order of 40 days (as for SST). For reaction times longer than 40 days it approaches -1 , as expected for a passive tracer advected by a two-dimensional turbulent field. The addition of turbulent diffusion significantly modifies the spectral slope of the tracers that react slowly, while those with reaction times shorter than the Lagrangian timescale (which is 16 days in the flow field considered) are almost unchanged. As a result, tracers with a reaction time of 20–40 days display a distribution with slopes comprised between -2.1 and -2.3 and limited variability at small scales, as observed for SST (see Figures 1 and 2). Results are summarized in Table 1. The spectra are averaged over five different time frames once the active scalar has reached statistical stationarity, and the slopes are calculated using the least squares fitting method.

3.2. Small-Scale Supply

[26] In this configuration, although unrealistic, the tracer supply is at small scale (~ 4 km). This scale still allows for a direct cascade of tracer variance to take place between $k = 64$ and $k \sim 110$. The supply scale is comparable to that by *Mahadevan and Campbell* [2002], but unlike in their study, is not correlated to the vorticity field. Similarly to the large-

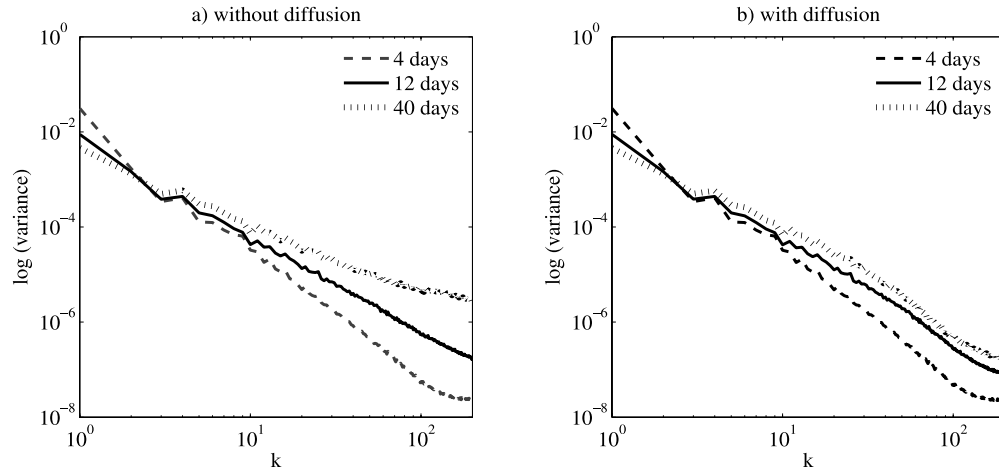


Figure 1. Spectra for the tracers with different reaction times upwelled at the large scale (a) without diffusion and (b) with diffusion.

scale supply case, in the absence of turbulent diffusion, the relaxation rate determines the spectral slope for each of the tracers. The spectral slopes are calculated in the inertial range (i.e., $k > 64$), because the tracers are not significantly influenced by the presence of an inverse energy cascade and evolve toward scales smaller than the forcing scale. For small R_t the slopes are generally steeper than those observed in the large-scale supply case (see Table 2). The general relationship between the reaction time and the spectral slope, however, remains unchanged compared to the large-scale input regime. The addition of turbulent diffusion does little to modify the distribution of the active scalars with values of R_t from a few days to a couple of weeks. For $R_t = 4$ days, the spectral slope with and without diffusion is -4.8 , while for a reaction time of two weeks the slopes are -3.0 and -3.2 , with and without diffusion, respectively. The greatest variations are again observed for the longest reaction time (40 days). In this case, the slope decreases from -1.25 to -1.9 once diffusion is added with the appropriate coeffi-

cient. This, however, is not enough to modify the relationship between the relative slopes for the various R_t values, and the general behavior suggested by *Abraham* [1998] is still in evidence.

3.3. Tracer Supply Inside Vortices and Filaments

[27] In the ocean tracer supply is linked to eddies, filaments and fronts [e.g., *Smith et al.*, 1996; *Spall and Richards*, 2000; *Martin et al.*, 2001; *Mahadevan and Campbell*, 2002; *McGillicuddy et al.*, 2003; *Levy and Klein*, 2004].

[28] In our simple model we can reproduce this situation by coupling the tracer supply to vortices and filaments, identified by large absolute values of the Okubo-Weiss parameter, OW [*Okubo*, 1970; *Weiss*, 1991]. In the absence of diffusion the spectral slope for the tracer depends more on the threshold value of the OW than on its reaction time. We selected three different thresholds for the absolute value of the Okubo-Weiss parameter above which supply takes place: 20, 10

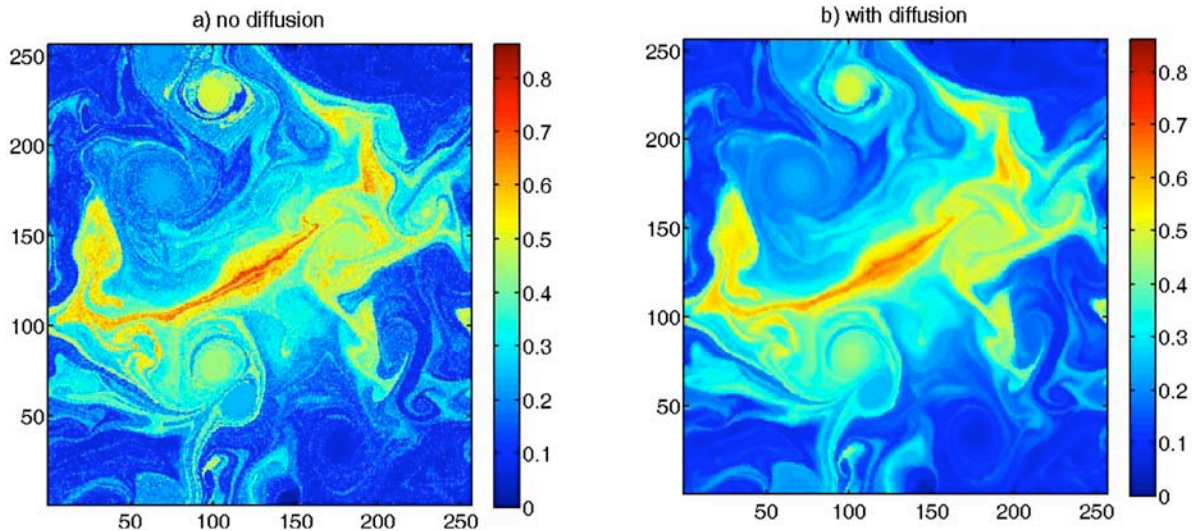


Figure 2. Distributions for the tracer with a reaction time $R_t = 40$ days (a) with a turbulent diffusivity coefficient of $0 \text{ m}^2 \text{ s}^{-1}$ and (b) with a coefficient of $1 \text{ m}^2 \text{ s}^{-1}$.

Table 1. Values for the Spectral Slopes of the Passive Tracer With Different Reaction Times and Turbulent Diffusivity Coefficients^a

Large-Scale Input, R_t (days)	λ (Turbulent Diffusivity Coefficient, in $\text{m}^2 \text{s}^{-1}$)			
	0.0	0.05	0.5	1
4	-2.5 ± 0.05	-2.5 ± 0.05	-2.5 ± 0.05	-2.6 ± 0.05
8	-2.3 ± 0.05	-2.32 ± 0.05	-2.5 ± 0.05	-2.6 ± 0.05
12	-2.1 ± 0.05	-2.13 ± 0.05	-2.35 ± 0.05	-2.47 ± 0.05
20	-1.7 ± 0.05	-1.75 ± 0.05	-2.2 ± 0.05	-2.3 ± 0.05
40	-1.3 ± 0.05	-1.44 ± 0.05	-1.95 ± 0.05	-2.1 ± 0.05

^aTracer is supplied to the model domain at the large scale.

and 5. In the absence of diffusion, when the tracer supply is limited to the core of the vortices ($OW < -20$) and the inner regions of the circulation cells surrounding them ($OW > 20$), spectral slopes between -1.75 and -1.85 are found for all reaction times at the scale of interest (Figure 3a and Table 3). The tracer is confined to regions completely impermeable to inward and outward fluxes and the background flow displays very low concentrations at all times. Lowering the threshold causes the upwelled tracer to occupy the edge of the vortices, the filaments and the whole circulation cells. Tracer contained at the edge of the coherent structures can mix more easily within the background flow, inducing small-scale patchiness, which results in a flattening of the spectral slope to values between -1.35 and -1.45 (see Figure 3b and Table 3). The recent analysis of vertical velocities in wind-forced anticyclones in a fully 3-D primitive equation model by *Koszalka* [2008] suggests that a lower threshold is a more realistic representation of the lateral extension of the upwelling induced by coherent vortices.

[29] In the presence of turbulent diffusion, tracers with a long reaction time diffuse more effectively within the vortices as well as in the background turbulence around them. Independent of the OW threshold, for $R_t = 40$ days and a sufficiently large diffusivity ($\geq 0.5 \text{ m}^2 \text{ s}^{-1}$), the spectral slopes varies little between -1.8 and -2 . When the Okubo-Weiss threshold is lowered from 20 to 5, slopes ranging from -1.75 to -1.35 , and -1.8 to -1.6 are found for $R_t = 4$ and 12 days, respectively (see Figure 4 and Table 3). Note that in presence of diffusion, the spectrum for a tracer with a reaction time comparable to that of zooplankton is slightly steeper than the one for a tracer representative of phytoplankton. In fact, in this case, the longer the tracer reaction time, the steeper the spectral slope, directly opposite to what happens when the tracer supply is uncorrelated with the flow. We verified that this also holds when the same value of diffusion is used for all of the tracers within the range explored in this work. Interestingly, comparable slopes were found by *Martin and Srokosz* [2002] in the North Atlantic in a region characterized by intense mesoscale variability. We speculate that the interplay between tracer reaction time,

advection by and within coherent vortices and filaments, and turbulent diffusion explains the observed slopes (see section 4).

3.4. PZ and NPZ Models

[30] Biological processes, as well as physical ones, have been suggested as generating mechanisms for plankton patchiness. So far, we have only considered a generic reactive tracer and the influence of physical processes on its distribution for different reaction times.

[31] In order to investigate whether biological interactions could significantly alter the results obtained so far, we start by using the simple PZ model described by equation (2) and introduced by *Abraham* [1998]. The addition of mortality and grazing terms does not alter the results for any of the configurations when the effective reaction time is considered. The effective reaction time can be calculated as $\langle R_t \rangle = \langle 1/P(Z) dP(Z)/dt \rangle$, i.e., the average time that phytoplankton (zooplankton) take to respond to a change in nutrient (phytoplankton) concentration. In the PZ model $\langle R_t \rangle$ is given, within a small error, by the growth rate for phytoplankton and by the maturation time for zooplankton. The quadratic mortality term for zooplankton contributes toward reducing the value of $\langle R_t \rangle$ with respect to the maturation time by roughly 1–2 days at most, for a broad range of mortality coefficients (see Figure 5 for a snapshot of the phytoplankton and zooplankton fields and their power spectra). When a more complex biological model is used, for instance that introduced by *Fasham et al.* [1990] presented in Appendix B, the results are confirmed but under the caveat that $\langle R_t \rangle$ is now linked in a more complex way to the terms of the equations. For zooplankton in particular, $\langle R_t \rangle$ is very small (roughly 2–3 days) and of the same order as the effective reaction time of phytoplankton, whenever the values of the parameters are in a range representative of open ocean regions (see Appendix B and *Martin et al.* [2002] for a further discussion of the parameter values). In the NPZ model, $\langle R_t \rangle$ for zooplankton is determined by the grazing term, strongly influenced by the phytoplankton growth rate and quite insensitive to the choice of assimilation efficiency. We performed a sensitivity analysis and found that in order to

Table 2. Values for the Spectral Slopes of the Passive Tracer With Different Reaction Times and Turbulent Diffusivity Coefficients^a

Small-Scale (4 km) Input, R_t (days)	λ (Diffusivity Coefficient, in $\text{m}^2 \text{s}^{-1}$)			
	0.0	0.05	0.5	1
4	-4.75 ± 0.05	-4.8 ± 0.05	-4.8 ± 0.05	-4.8 ± 0.05
12	-3.0 ± 0.05	-3.0 ± 0.05	-3.1 ± 0.05	-3.2 ± 0.05
40	-1.25 ± 0.05	-1.4 ± 0.05	-1.75 ± 0.05	-1.9 ± 0.05

^aTracer is supplied to the model domain in 64 small patches.

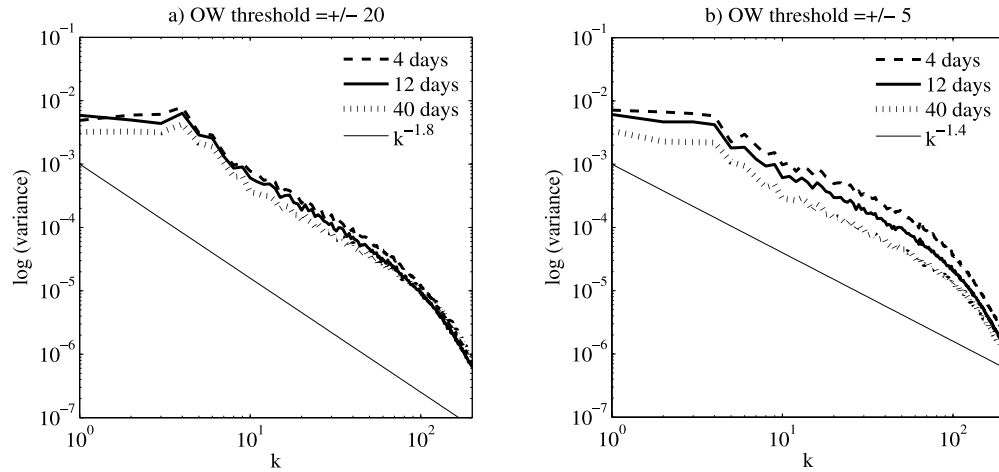


Figure 3. Spectra for the tracers in the case of tracer supply coupled to vortices with different thresholds of the Okubo-Weiss parameter OW and no diffusion. (a) OW threshold = ± 20 and (b) OW threshold = ± 5 . The slope that better fits the variance of the tracer with a reaction time $R_r = 12$ days (intermediate case, solid line) is also shown.

recover an effective reaction time for zooplankton of the order of a week and power spectra analogous to that described for the simple tracer equation, we had to (1) adopt an unrealistically small assimilation efficiency, i.e., less than 0.15; (2) introduce an ad hoc delay in the zooplankton maturation time, as in *Abraham's* [1998] PZ model; or (3) assume a minimum phytoplankton concentration at which grazing can occur.

4. Discussion and Conclusions

[32] In this study, we investigated the impact of the spatial scale of tracer supply, the role played by coherent vortices, and the role of diffusion in determining the distribution of a reactive tracer at the ocean surface. We adopted a simple barotropic turbulent advection field and focused on tracers with reaction times representative, in the ocean, of temperature (40 days), zooplankton (12 days) and phytoplankton (4 days). Our results suggest that turbulent diffusion is the dominant process determining the spectral distribution of tracers with a reaction time longer than the Lagrangian decorrelation timescale (i.e., longer than a couple of weeks), as in the case of SST. Regardless of the supply regime, once diffusion is added to the model, a tracer with a reaction time comparable to that of SST exhibits a spectral slope between -1.8 and -2.3 , which is in line with observed values and indicates a relatively large degree of homogenization.

[33] When the tracer supply is uncorrelated with the flow field, at small or large scales, the relationship between tracers with different reaction times is determined by the reaction timescale. The faster the reaction time, the steeper the spectral slope of the tracer distribution, suggesting that the tracer has little time to cascade to small scales before being consumed, in agreement with the results of *Abraham* [1998]. This would suggest that the scale of the tracer supply, per se, is not fundamental in determining the relative slopes of tracer spectra where there is sufficient space for a direct cascade. Diffusion, within values reasonable for the upper ocean, significantly reduces the small-scale variability of tracers with a reaction time of the order of a week or

longer, but only minimally impacts tracers reacting on a scale of a few days. In this latter case, the reaction timescale is several times faster than the diffusion timescale and, thus, determines the spectral slope. Diffusion thereby contributes to reducing the differences between the distributions of phytoplankton and zooplankton. When the supply is coupled to the coherent structures in the flow (vortices and filaments in our model), the resulting tracer distributions are very different from the previous cases. In the absence of diffusion, a single process, not strongly affected by the reaction time of the tracers, is dominant in generating the observed distributions. This is, in fact, the lifetime of the coherent structures which are trapping the tracers and acting as transport barriers. The eddy lifetime, usually measured in months rather than days, is longer than the timescales of all of the other processes which come into play in this problem, and sets the spectral slopes of the tracer concentrations almost independently of the reaction time. In presence of diffusion, tracers with long reaction times are characterized by spectra steeper than those of tracers with shorter reaction times, because they are given more time to reach a relatively high degree of homogenization. This may explain the steeper zooplankton than phytoplankton spectra observed in regions of intense eddy activity [*Martin and Srokosz*, 2002] and the

Table 3. Values for the Spectral Slopes of the Passive Tracer With Different Reaction Times and Diffusivity Coefficients^a

R_r (days)	λ (Diffusivity Coefficient, in $m^2 s^{-1}$)			
	0.0	0.05	0.5	1
<i>OW Threshold ± 20</i>				
4	-1.75 ± 0.05	-1.75 ± 0.05	-1.78 ± 0.05	-1.80 ± 0.05
12	-1.75 ± 0.05	-1.75 ± 0.05	-1.80 ± 0.05	-1.92 ± 0.05
40	-1.90 ± 0.05	-1.95 ± 0.05	-2.0 ± 0.05	-2.0 ± 0.05
<i>OW Threshold ± 5</i>				
4	-1.35 ± 0.05	-1.35 ± 0.05	-1.35 ± 0.05	-1.38 ± 0.05
12	-1.4 ± 0.05	-1.45 ± 0.05	-1.6 ± 0.05	-1.7 ± 0.05
40	-1.45 ± 0.05	-1.55 ± 0.05	-1.8 ± 0.05	-1.95 ± 0.05

^aTracer is supplied inside vortices and filaments and for two values of the Okubo-Weiss threshold.

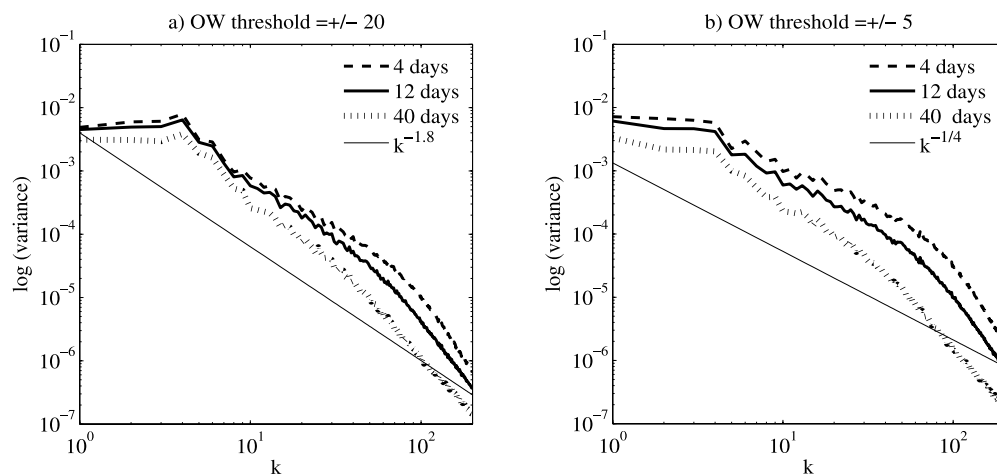


Figure 4. Spectra for the tracers supplied in the vortices as in Figure 3 but in presence of diffusion. (a) OW threshold = ± 20 and (b) OW threshold = ± 5 . The same slopes shown in Figure 3 are plotted for comparison.

finding that SST distributions in frontal regions have less small-scale variance than chlorophyll [Mahadevan and Campbell, 2002]. When planktonic distributions are associated with mesoscale upwelling of nutrients, in vortices and filaments, as in this work, or in frontal regions, as in the paper by Mahadevan and Campbell [2002], i.e., when the nutrient upwelling is correlated with transport barriers, the relationship between the slopes for phytoplankton and zooplankton may differ depending on the level of turbulence in the ocean, as well as biological interactions. If the biological activity is tightly coupled to upwelling events within and around transport barriers, the relatively long reaction time of zooplankton might be large enough for diffusion to homogenize the concentration across the front or the edge of the eddy. The phytoplankton reaction time is shorter, so the phytoplankton spectrum will remain unaffected by turbulent diffusion, resulting in a flatter spectral slope for phytoplankton than for zooplankton. Conversely, when the biological activity is not correlated with the presence of coherent structures, as in the case of large spring blooms, the phytoplankton spectrum will be steeper than for zooplankton, because its shorter reaction time prevents the cascade from reaching small scales.

[34] The introduction of more complex models to describe planktonic dynamics at the ocean surface does not alter the above conclusions when an effective reaction time, $\langle R_t \rangle$, is considered. $\langle R_t \rangle$ can be calculated by postprocessing the numerical results in our simple integrations, but may not be so easily determined in the presence of 3-D advection. The effective reaction time is intrinsically linked to the mathematical description of biological interactions in the ecosystem model considered. In the standard model introduced by Fasham *et al.* [1990] phytoplankton and zooplankton have almost identical $\langle R_t \rangle$ for realistic sets of parameters, thus implying that very similar spectral slopes for the planktonic distributions will be obtained with this ecosystem model. The simpler ecosystem model proposed by Abraham [1998], on the other hand, maintains different $\langle R_t \rangle$ with the introduction of an explicit delay term in the zooplankton response to changes in phytoplankton concentration, and thereby guar-

antees different slopes when the nutrient supply (or carrying capacity) is not correlated with the flow field, as in the case of mixed layer deepening or large-scale upwelling.

[35] Our results generalize the work by Srokosz *et al.* [2003], which focused on the origin of plankton patchiness in the eastern North Atlantic. Analyzing field data they found that the patchiness of the plankton distributions was, in fact, determined by physical processes, while the biological dynamics controlled the size of the populations within the structures and the relationship between phytoplankton and zooplankton concentrations. Here we have shown that the interplay between diffusion and the direct turbulent cascade determines the plankton distributions when the supply of nutrients is uncorrelated with the flow field. The cascade of variance from large to small scales sets the relative slope of the power spectra. On the other hand, diffusion and the impermeability of the coherent structures (vortices and filaments in our model) to inward and outward fluxes determine the level of patchiness when the tracer supply is correlated with the vorticity field. In this latter case, diffusion across the transport barriers can cause a reversal of the general relationship observed in association with the direct turbulent cascade, and tracers with a shorter reaction time and smaller effective diffusivity, may maintain a greater variance at small scales.

[36] To conclude, this study has shown that the distribution of a reactive tracer at the ocean surface is definitely dependent on how the tracer is supplied to the euphotic layer. Here we prescribe this supply and, in the case of supply correlated with the coherent structures, we assume that a simple relationship between strain and vorticity fields and vertical velocities exists. This is a major limitation of our results. Recent literature points to the importance of ageostrophic contributions to the vertical velocities within and around vortices and fronts [e.g., Mahadevan and Tandon, 2006; Capet *et al.*, 2008; Klein *et al.*, 2008; Koszalka, 2008]. In our opinion, the main open issue is therefore to understand the role of the ageostrophic component of the vertical velocities to the submesoscale input

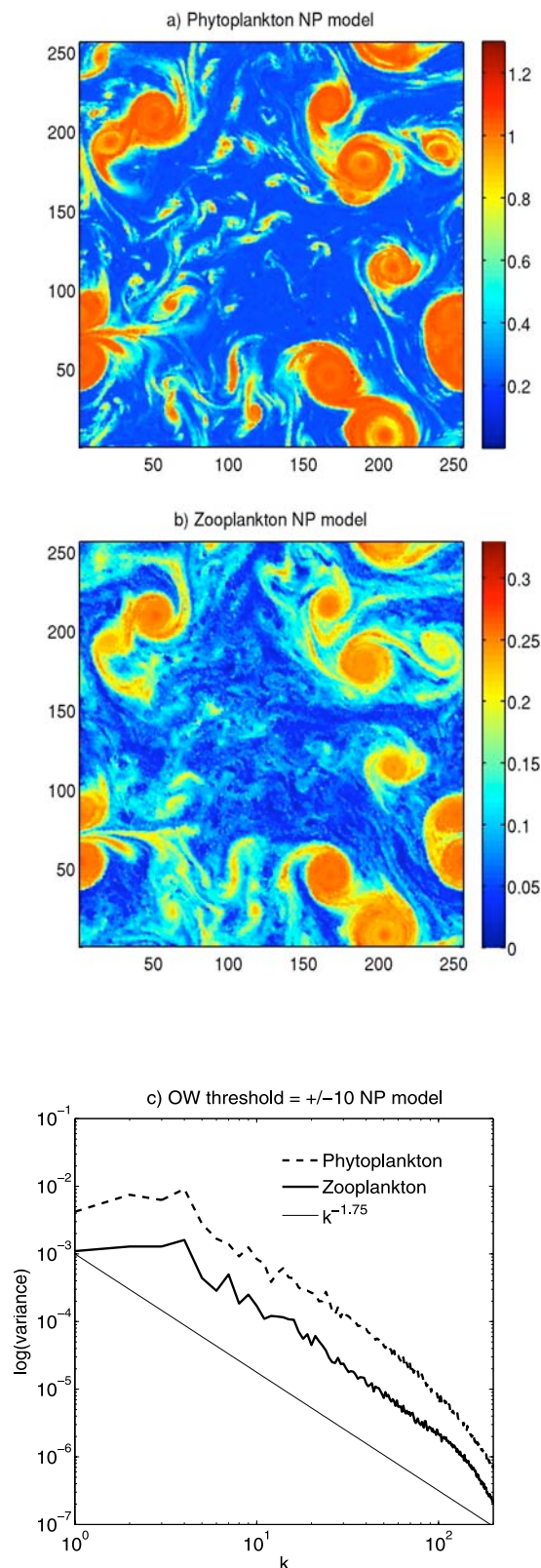


Figure 5. Snapshots of the fields of phytoplankton and zooplankton obtained with the PZ model proposed by Abraham [1998], configured with the carrying capacity coupled to the vortices with a threshold in the Okubo-Weiss parameter $OW = \pm 10$ and in presence of diffusion. (a) Snapshot of the phytoplankton distribution, (b) snapshot of zooplankton, and (c) power spectra for the two tracers (single snapshot).

(output) of nutrients to (from) the euphotic layer. We plan to address this point in future studies.

Appendix A

[37] Solving the advection-reaction-diffusion equation for biogeochemical tracers, either analytically or numerically, is particularly time consuming. Additionally, it is difficult to fully control diffusion processes, as numerical schemes usually adopted in the context of biogeochemical modeling introduce spurious diffusive contributions to secure positive values to the tracer concentrations (see Lévy *et al.* [2001a] for a comparison of five different advection schemes and a more in-depth discussion of this point). In this study we adopt a Lagrangian approach to the numerical integration of the equations governing the behavior of the various tracers, in order to avoid the difficulties encountered with the Eulerian formulation. This approach, already adopted by Abraham [1998] is described in detail by Pasquero *et al.* [2004]. The advecting flow field is obtained from the Eulerian numerical integration of the momentum equation (equation (1)). The advection-reaction-diffusion equations, however, are not solved for in their Eulerian form. The reactions are computed for each of a large number (512^2) of independent, tracer-carrying fluid elements, advected by the turbulent flow described in equation (1). Each fluid parcel represents a given water volume (whose size is comparable to that of the grid cells used to integrate the Eulerian momentum equations), assumed to have homogeneous properties. The tracer reactions occur within each fluid parcel, and do not depend on the tracer concentrations in the neighboring parcels, allowing for the formation of sharp gradients. In order to obtain a concentration field, the distribution of the Lagrangian particles are then interpolated onto a regular grid and a tracer field obtained.

[38] The diffusion of properties between fluid parcels is represented by introducing a mixing term for neighboring fluid parcels: consider two water parcels, i and j , at distance r_{ij} from each other, with concentration C_i and C_j , respectively. Mixing is introduced by assuming that there is a flux of the tracer component toward the fluid parcel with the lower tracer concentration. At each step of the integration, the mixing law is given by $C_{i, \text{mixed}} = C_i + h(r_{ij})(C_j - C_i)$ for any two fluid parcels, i and j , closer to each other than a given threshold. The weight function is $h(r) = \alpha \exp(-r^2/r_0^2)$, where r_0 measures the scale of mixing. This type of mixing law provides the closest representation of Fick's law in the Lagrangian framework we could find. In order to specify the threshold distance α and r_0 , it was required the concentration fields obtained for a subset of 12 integrations in the Lagrangian framework for the simple tracer described by equation (2a), in various supply configurations, to be analogous to those obtained integrating the Eulerian reaction-advection-diffusion equation in the same configurations, in presence of a Fickian diffusion term. The tracer concentration field obtained in the Lagrangian approach and interpolated on a regular grid was considered analogous to the Eulerian outcome if the spectral slopes obtained by least squares fitting were the same and the point-to-point differences in concentration did not exceed 5%. In order to avoid spurious negative concentrations, caused by numerical noise and spectral wiggles, without introducing any ad hoc positive concentra-

Table B1. List of Parameters Used in the NPZ Biological Model

Parameter	Definition	Value
β	Maximum phytoplankton growth rate	0.66 d ⁻¹
γ	Assimilation efficiency	0.75
ε	Prey capture rate	1.0 (mmol N m ⁻³) ⁻² d ⁻¹
α	Maximum grazing rate	2.0 d ⁻¹
k_N	Half saturation constant for N uptake	0.5 mmol N m ⁻³
μ_N	Regeneration efficiency	0.2
μ_P	Phytoplankton mortality coefficient	0.03 d ⁻¹
μ_Z	Zooplankton mortality coefficient	0.2 (mmol N m ⁻³) ⁻¹ d ⁻¹

tion preserving advection scheme, we simply set to zero any (small) negative value we encountered in the Eulerian runs. This, in general, cannot be done with more sophisticated reaction equations, because the error introduced becomes significant. For the simple reaction described in equation (2a) the number of points subject to this correction was small and inversely proportional to the diffusion rate (O(1) points over 512² were affected at each time step for diffusion coefficients $\geq 0.5 \text{ m}^2 \text{ s}^{-1}$; Eulerian runs in the absence of diffusion or with a very small diffusion coefficient cannot, on the other hand, be performed because of the numerical noise dominating the small-scale dynamics).

[39] As a note of caution, it should be kept in mind that the Lagrangian approach requires that the biological components of the model do not swim. This is an appropriate assumption for phytoplankton and zooplankton at the mesoscale and larger scales, where the horizontal size of the advected fluid parcels is of the order of 200 km. At these scales, phytoplankton and zooplankton act as passive tracers.

Appendix B

[40] The Nutrient-Phytoplankton-Zooplankton (NPZ) model used to confirm our findings integrates the following equations:

$$\frac{dN}{dt} = f(N, P, Z) + \lambda \nabla^2 N = \Theta - \beta \frac{N}{k_N + N} + \mu_N \left[(1 - \gamma) \frac{\alpha \varepsilon P^2}{\alpha + \varepsilon P^2} Z + \mu_P P + \mu_Z Z^2 \right] + \lambda \nabla^2 N, \quad (\text{B1a})$$

$$\frac{dP}{dt} = g(N, P, Z) + \lambda' \nabla^2 P = \beta \frac{N}{k_N + N} - \frac{\alpha \varepsilon P^2}{\alpha + \varepsilon P^2} Z - \mu_P P + \lambda' \nabla^2 P, \quad (\text{B1b})$$

$$\frac{dZ}{dt} = h(N, P, Z) + \lambda'' \nabla^2 Z = \gamma \frac{\alpha \varepsilon P^2}{\alpha + \varepsilon P^2} Z - \mu_Z Z^2 + \lambda'' \nabla^2 Z, \quad (\text{B1c})$$

where nutrient (N), phytoplankton (P) and zooplankton (Z) variables represent averaged concentrations in the surface mixed layer. The reader is referred to *Oschlies and Garçon* [1999] for a detailed description of the model.

[41] The terms on the right-hand side of the equation for the nutrient represent nutrient supply (Θ), the conversion of nutrient into organic matter through phytoplankton activity,

and the regeneration of dead organic matter into nutrients, respectively. The regeneration efficiency, μ_N , is smaller than unity, as not all biological material is available as a nutrient, and part is lost by detritus sinking to deeper waters. Phytoplankton dynamics are regulated by production, grazing by zooplankton, and linear mortality. Zooplankton grow when phytoplankton are present with an assimilation efficiency γ , and die according to a quadratic mortality term. The parameter values typical of midlatitude subeuphotic concentrations are reported in Table B1.

[42] **Acknowledgments.** Sincerest thanks to Francesco Paparella for stimulating discussions and for providing us with a properly functional code to interpolate the fluid particles into a regular grid. Thanks also to two anonymous reviewers and the JGR associate editor for their constructive comments which helped improve the initial paper. This work was initiated at WHOI during the summer of 2006, while S.C. was a summer student fellow, partially funded by the NSF. A.B. is funded by NSF–OCE 0751775 and NSF–OCE 0815280, and C.P. is funded by NSF–PHY 0551164.

References

- Abraham, E. R. (1998), The generation of plankton patchiness by turbulent stirring, *Nature*, *391*, 577–580, doi:10.1038/35361.
- Armi, L., and P. Flament (1985), Cautionary remarks on the spectral interpretation of turbulent flows, *J. Geophys. Res.*, *90*, 11,779–11,782, doi:10.1029/JC090iC06p11779.
- Bracco, A., A. Provenzale, and I. Scheuring (2000a), Mesoscale vortices and the paradox of the plankton, *Proc. R. Soc. London, Ser. B*, *267*, 1795–1800, doi:10.1098/rspb.2000.1212.
- Bracco, A., J. LaCasce, and A. Provenzale (2000b), Velocity probability density functions for oceanic floats, *J. Phys. Oceanogr.*, *30*, 461–474, doi:10.1175/1520-0485(2000)030<0461:VPDFFO>2.0.CO;2.
- Bracco, A., J. LaCasce, C. Pasquero, and A. Provenzale (2000c), Velocity PDFs in barotropic turbulence, *Phys. Fluids*, *12*, 2478–2488, doi:10.1063/1.1288517.
- Bracco, A., J. von Hardenberg, A. Provenzale, J. Weiss, and J. C. McWilliams (2004), Dispersion and mixing in quasisubgeostrophic turbulence, *Phys. Rev. Lett.*, *92*, 084501, doi:10.1103/PhysRevLett.92.084501.
- Capet, X., J. C. McWilliams, M. J. Molemaker, and A. Shchepetkin (2008), The transition from mesoscales to submesoscale in the California Current System: Frontal processes, *J. Phys. Oceanogr.*, *38*, 44–64, doi:10.1175/2007JPO3672.1.
- Denman, K., A. Okubo, and T. Platt (1977), The chlorophyll fluctuation spectrum in the sea, *Limnol. Oceanogr.*, *22*, 1033–1038.
- Elhmaïdi, D., A. Provenzale, and A. Babiano (1993), Elementary topology of two-dimensional turbulence from a Lagrangian viewpoint and single-particle dispersion, *J. Fluid Mech.*, *257*, 533–558, doi:10.1017/S0022112093003192.
- Falkowski, P. G., Z. Kolber, D. Ziemann, and P. K. Bienfang (1991), Role of eddy pumping in enhancing primary production in the ocean, *Nature*, *352*, 55–58, doi:10.1038/352055a0.
- Fasham, M. J. R., H. W. Ducklow, and S. M. McKelvie (1990), A nitrogen-based model of plankton dynamics in the oceanic mixed layer, *J. Mar. Res.*, *48*, 591–639.
- Folt, C. L., and C. W. Burns (1999), Biological drivers of zooplankton patchiness, *Trends Ecol. Evol.*, *14*(8), 300–305, doi:10.1016/S0169-5347(99)01616-X.
- Gower, J. F. R., K. L. Denman, and R. J. Holyer (1980), Phytoplankton patchiness indicates the fluctuation spectrum of mesoscale oceanic structure, *Nature*, *288*, 157–159, doi:10.1038/288157a0.
- Horwood, J. (1981), Variation of fluorescence, particle-size groups, and environmental parameters in the Southern North Sea, *ICES J. Mar. Sci.*, *39*(3), 261–270, doi:10.1093/icesjms/39.3.261.
- Klein, P., B. L. Hua, G. Lapyere, X. Capet, S. Le Gentil, and H. Sasaki (2008), Upper ocean turbulence from high 3D resolution simulations, *J. Phys. Oceanogr.*, *38*, 1748–1763.
- Koszalka, I. (2008), Mesoscale vortices, Lagrangian transport and marine ecosystem dynamics, Ph.D. thesis, 104 pp., Politecnico di Torino, Turin, Italy.
- Ledwell, J. R., A. J. Watson, and C. S. Law (1998), Mixing of a tracer in the pycnocline, *J. Geophys. Res.*, *103*, 21,499–21,530, doi:10.1029/98JC01738.
- Levin, S. A., A. Morin, and T. H. Powell (1989), Patterns and processes in the distribution and dynamics of Antarctic krill, in *Selected Scientific Papers Part 1, Rep. SC-CAMLR-SSP/5*, pp. 281–299, Comm. for the Conserv. of Antarct. Mar. Living Resour., Hobart, Australia.

- Levy, M., and P. Klein (2004), Does the low frequency variability of meso-scale dynamics explain a part of the phytoplankton and zooplankton spectral variability?, *Proc. R. Soc. London, Ser. A*, *460*, 1673–1687.
- Lévy, M., A. Estubier, and G. Madec (2001a), Choice of an advection scheme for biogeochemical models, *Geophys. Res. Lett.*, *28*, 3725–3728, doi:10.1029/2001GL012947.
- Lévy, M., P. Klein, and A. M. Treguier (2001b), Impact of sub-mesoscale physics on production and subduction of phytoplankton in an oligotrophic regime, *J. Mar. Res.*, *59*, 535–565, doi:10.1357/002224001762842181.
- Mackas, D. L., and C. M. Boyd (1979), Spectral analysis of zooplankton heterogeneity, *Science*, *204*, 62–64, doi:10.1126/science.204.4388.62.
- Mahadevan, A., and D. Archer (2000), Modeling the impact of fronts and mesoscale circulation on the nutrient supply and biogeochemistry of the upper ocean, *J. Geophys. Res.*, *105*, 1209–1226, doi:10.1029/1999JC900216.
- Mahadevan, A., and J. W. Campbell (2002), Biogeochemical patchiness at the sea surface, *Geophys. Res. Lett.*, *29*(19), 1926, doi:10.1029/2001GL014116.
- Mahadevan, A., and A. Tandon (2006), An analysis of mechanisms for submesoscale vertical motion at ocean fronts, *Ocean Modell.*, *14*, 241–256, doi:10.1016/j.ocemod.2006.05.006.
- Martin, A. P., and K. J. Richards (2001), Mechanisms for vertical transport within a North Atlantic mesoscale eddy, *Deep Sea Res., Part II*, *48*, 757–773.
- Martin, A. P., and M. A. Srokosz (2002), Plankton distribution spectra: Inter-size class variability and the relative slopes for phytoplankton and zooplankton, *Geophys. Res. Lett.*, *29*(24), 2213, doi:10.1029/2002GL015117.
- Martin, A. P., K. J. Richards, and M. J. R. Fasham (2001), Phytoplankton production and community structure in an unstable frontal region, *J. Mar. Syst.*, *28*, 65–89, doi:10.1016/S0924-7963(00)00084-1.
- Martin, A. P., K. J. Richards, A. Bracco, and A. Provenzale (2002), Patchy productivity in the open ocean, *Global Biogeochem. Cycles*, *16*(2), 1025, doi:10.1029/2001GB001449.
- McGillicuddy, D. J., and A. R. Robinson (1997), Eddy-induced nutrient supply and new production in the Sargasso Sea, *Deep Sea Res., Part I*, *44*, 1427–1450, doi:10.1016/S0967-0637(97)00024-1.
- McGillicuddy, D. J., A. R. Robinson, D. A. Siegel, H. W. Jannasch, R. Johnson, T. D. Dickey, J. McNeil, A. F. Michaels, and A. H. Knap (1998), Influence of mesoscale eddies on new production in the Sargasso Sea, *Nature*, *394*, 263–266, doi:10.1038/28367.
- McGillicuddy, D. J., L. A. Anderson, S. C. Doney, and M. E. Maltrud (2003), Eddy-driven sources and sinks of nutrients in the upper ocean: Results from a 0.1 degree resolution model of the North Atlantic, *Global Biogeochem. Cycles*, *17*(2), 1035, doi:10.1029/2002GB001987.
- McGillicuddy, D. J., et al. (2007), Eddy/wind interactions stimulate extraordinary mid-ocean plankton blooms, *Nature*, *316*, 1021–1026.
- Okubo, A. (1970), Horizontal dispersion of floatable particles in the vicinity of velocity singularities such as convergences, *Deep Sea Res.*, *17*, 445–454.
- Oschlies, A., and V. Garçon (1998), Eddy-induced enhancement of primary production in a model of the North Atlantic Ocean, *Nature*, *394*, 266–269, doi:10.1038/28373.
- Oschlies, A., and V. Garçon (1999), An eddy-permitting coupled physical-biological model of the North Atlantic I. Sensitivity to advection numerics and mixed layer physics, *Global Biogeochem. Cycles*, *13*, 135–160, doi:10.1029/98GB02811.
- Park, S., C. Deser, and M. A. Alexander (2005), Estimation of surface heat fluxes response to sea surface temperature anomalies over the global oceans, *J. Clim.*, *18*, 4582–4599, doi:10.1175/JCLI3521.1.
- Pasquero, C. (2005), Differential eddy diffusion of biogeochemical tracers, *Geophys. Res. Lett.*, *32*, L17603, doi:10.1029/2005GL023662.
- Pasquero, C., A. Bracco, and A. Provenzale (2004), Coherent vortices, Lagrangian particles and the marine ecosystem, in *Shallow Flows*, edited by G. H. Jirka and W. S. J. Uijtewaal, pp. 399–412, A. A. Balkema, Leiden, Netherlands.
- Pasquero, C., A. Bracco, and A. Provenzale (2005), Impact of the spatio-temporal variability of the nutrient flux on primary productivity in the ocean, *J. Geophys. Res.*, *110*, C07005, doi:10.1029/2004JC002738.
- Piontkovski, S. A., R. Williams, W. T. Peterson, O. A. Yunev, N. I. Minkina, V. L. Vladimirov, and A. Blinkov (1997), Spatial heterogeneity of the planktonic fields in the upper mixed layer of the open ocean, *Mar. Ecol. Prog. Ser.*, *148*, 145–154, doi:10.3354/meps148145.
- Platt, T. (1972), Local phytoplankton abundance and turbulence, *Deep Sea Res.*, *19*, 183–187.
- Plumb, R. (1979), Eddy fluxes of conserved quantities by small-amplitude waves, *J. Atmos. Sci.*, *36*, 1699–1704, doi:10.1175/1520-0469(1979)036<1699:EFQCQB>2.0.CO;2.
- Polzin, K. L. (2003), Idealized solutions for the energy balance of the fine-scale internal wave field, *J. Phys. Oceanogr.*, *34*, 231–246, doi:10.1175/1520-0485(2004)034<0231:ISFTEB>2.0.CO;2.
- Polzin, K. L., and R. Ferrari (2004), Isopycnal dispersion in NATRE, *J. Phys. Oceanogr.*, *34*, 247–257, doi:10.1175/1520-0485(2004)034<0247:IDIN>2.0.CO;2.
- Powell, T. M., and A. Okubo (1994), Turbulence, diffusion and patchiness in the sea, *Philos. Trans. Biol. Sci.*, *343*, 11–18, doi:10.1098/rstb.1994.0002.
- Provenzale, A. (1999), Transport by coherent barotropic vortices, *Annu. Rev. Fluid Mech.*, *31*, 55–93, doi:10.1146/annurev.fluid.31.1.55.
- Richards, K. J., and S. J. Brentnall (2006), The impact of diffusion and stirring on the dynamics of interacting populations, *J. Theor. Biol.*, *238*, 340–347.
- Salmon, R. L. (1998), *Lectures on Geophysical Fluid Dynamics*, Oxford Univ. Press, Oxford, U. K.
- Schorghofer, N. (2000), Universality of probability distributions among two-dimensional turbulent flows, *Phys. Rev. E*, *61*, 6568–6571, doi:10.1103/PhysRevE.61.6568.
- Siegel, D. A., E. Fields, and D. J. McGillicuddy Jr. (1999), Mesoscale motions, satellite altimetry and new production in the Sargasso Sea, *J. Geophys. Res.*, *104*, 13,359–13,379, doi:10.1029/1999JC900051.
- Smith, C., K. J. Richards, and M. J. Fasham (1996), The impact of mesoscale eddies on plankton dynamics in the upper ocean, *Deep Sea Res., Part I*, *43*, 1807–1832, doi:10.1016/S0967-0637(96)00035-0.
- Spall, S. A., and K. J. Richards (2000), A numerical model of mesoscale frontal instabilities and plankton dynamics — I. Model formulation and initial experiments, *Deep Sea Res., Part I*, *47*, 1261–1301, doi:10.1016/S0967-0637(99)00081-3.
- Srokosz, M. A., A. P. Martin, and M. J. R. Fasham (2003), On the role of biological dynamics in plankton patchiness at the mesoscale: An example from the eastern North Atlantic Ocean, *J. Mar. Res.*, *61*, 517–537, doi:10.1357/002224003322384915.
- Steele, J. (1974), Spatial heterogeneity and population stability, *Nature*, *248*, 83, doi:10.1038/248083a0.
- Sundermeyer, M. A., and J. F. Price (1998), Lateral mixing and the North Atlantic Tracer Release Experiment: Observations and simulations of Lagrangian particles and a passive tracer, *J. Geophys. Res.*, *103*, 21,481–21,497, doi:10.1029/98JC01999.
- Tsuda, A., H. Sugisaki, T. Ishimaru, T. Saino, and T. Sato (1993), White-noise-like distribution of the oceanic copepod *Neocalanus cristatus* in the subarctic North Pacific, *Mar. Ecol. Prog. Ser.*, *97*, 39–46, doi:10.3354/meps097039.
- Weber, L. H., S. Z. El-Sayed, and I. Hampton (1986), The variance spectra of phytoplankton, krill and water temperature in the Atlantic Ocean south of Australia, *Deep Sea Res., Part A*, *33*, 1327–1343, doi:10.1016/0198-0149(86)90039-7.
- Weiss, J. (1991), The dynamics of enstrophy transfer in two-dimensional hydrodynamics, *Physica D*, *48*, 273–294, doi:10.1016/0167-2789(91)90088-Q.

A. Bracco, EAS-CNS, Georgia Institute of Technology, Atlanta, GA 30332, USA. (abracco@gatech.edu)

S. Clayton, MIT/WHOI Joint Program in Oceanography, Department of Physical Oceanography, Woods Hole Oceanographic Institution, Woods Hole, MA 02543, USA.

C. Pasquero, Department of Earth System Science, University of California, Irvine, CA 92697-3100, USA.